Prediction of a Dirac state in monolayer TiB_{2}

L. Z. Zhang, Z. F. Wang, S. X. Du, H.-J. Gao, and Feng Liu

Phys. Rev. B **90**, 161402 — Published 3 October 2014

DOI: 10.1103/PhysRevB.90.161402

Prediction of Dirac state in monolayer TiB_2

L. Z. Zhang,[1,2] Z. F. Wang,[2] S. X. Du,[1,*] H.-J. Gao,[1] F. Liu [2,3,†]
[1] *Institute of Physics, Chinese Academy of Sciences, Beijing 100190, China*
[2] *Department of Materials Science and Engineering, University of Utah, Salt Lake City, UT 84112, USA*
[3] *Collaborative Innovation Center of Quantum Matter, Beijing 100871, China*

We predict the existence of Dirac state in monolayer TiB_2 sheet (m-TiB_2), a two-dimensional metal diboride, based on first-principles calculations. Band structure of m-TiB_2 is found to be characterized with anisotropic Dirac cones with the largest Fermi velocity of 0.57×10^6 m/s, which is about one-half of that of graphene. The Dirac point is located at the Fermi level between K and Γ point, with Dirac states arising primarily from d orbitals of Ti. Freestanding m-TiB_2 exhibits a bending instability, so that a planar m-TiB_2 needs to be stabilized on a substrate. Calculation of m-TiB_2 on h-BN substrate reveals a negligible influence of the h-BN substrate to the electronic properties of m-TiB_2. Our findings extend the Dirac materials to metal diborides.

PACS numbers: 61.46.-w, 68.55.-a, 73.22.-f

Graphene, due to its special two equivalent carbon sublattices in the honeycomb structure, has massless carriers which can be described by the Dirac equations and called Dirac fermions.[1] Such Dirac materials with a linear band dispersion around the Fermi level, display ballistic charge transport and enormously high carrier mobility.[1] Since the Dirac fermions was first observed in graphene,[1–3] Dirac states have been proposed and studied in many other Dirac materials. These include molecular graphene,[4] janugraphene and chlorographene,[5] α- and β-graphyne,[6] strongly bond G/i-TM/SiC,[7] surface of topological insulators,[8] silicene and germanene,[9] Pmmn boron,[10] and two-dimensional (2-D) organic topological insulators[11]. The search for Dirac materials has been ongoing. Especially, it is interesting to go beyond the carbonic and topological materials.

Boron, as the neighbor of carbon in the periodic table, has attracted enormous interest during the past few years.[10,12,13] Due to its open electron shell structure (one electron short of being half-filled), B can easily bind with transition metal atoms. Up to now, many metal-boron nanostructures have been predicted, including nanotubes[14–17] and nanosheets.[18–20] Especially in a planar metal-diboride structure, such as BeB_2, B atoms form a hexagonal lattice like graphene and Be atoms provide the missing valence electrons. As such, the charge arrangements in the B layer are very similar to graphene, suggesting a high structural stability. [17] This metal doping mechanism can be extended to other metal-diboride systems, whose electronic properties can be turned by using different metals.[18–20] Experimentally, formation of multilayer MgB_2 sheets on Mg(0001) surface[21] and multilayer TiB_2 sheets at the interface of TiC and B_4C have been reported.[22]

In this Rapid Communication, we investigate the electronic properties and stability of monolayer TiB_2 sheet (m-TiB_2) by using first-principles calculations. We find that m-TiB_2 turns out to be a Dirac material, exhibits Dirac cones near the Fermi level (E_F), characterized with a Fermi velocity about one-half of that of graphene. Different from p-orbital Dirac state in graphene, the Dirac states in m-TiB_2 are of d-orbital character, arising predominantly from the d orbitals of Ti. The Dirac points are located at off-symmetry points in between K and Γ. Importantly, we point out that freestanding m-TiB_2 exhibits a bending instability so that a planar m-TiB_2 needs to be stabilized on a substrate. Calculation of m-TiB_2 on h-BN substrate shows that the Dirac states are retained on the h-BN substrate.

All density functional theory calculations are carried by using Vienna ab-initio simulation package (VASP)[23,24] with the projector augmented wave method.[25] Local density approximation[26] in the form of Perdew-Zunger[27] is adopted for the exchange-correlation function. The energy cutoff of the plane-wave basis sets is 400 eV. The Monkhorst-Pack scheme with $27 \times 27 \times 1$ k-points is used to sample the Brillouin zone. For the model containing 4×4 m-TiB_2 on 5×5 h-BN, a $9 \times 9 \times 1$ k-points sampling is used, and the whole h-BN substrate is fixed. For the calculations of the TiB_2 nanotubes, the $1 \times 1 \times 27$ k-points sampling is used. In all the calculations, a 15 $\mathring{A}$ vacuum layer is used and all atoms are fully relaxed in geometric optimizations until the residual forces on each atom are smaller than 0.01 $eV/\mathring{A}$. The phonon frequencies are calculated by using a supercell approach as implemented in the PHONOPY code.[28,29]

Figure 1(a) shows the top and side view of the optimized structures of m-TiB_2 in a presumed planar structure. One unit cell contains two B atoms and one Ti atom. B atoms arrange in a honeycomb lattice, Ti atoms locate in the middle of the hexagons. This monolayer sheet can be considered as one layer cutting from the bulk TiB_2 or the Ti adsorbed graphene-like B sheet. The B-B bond length, l_{B-B} is 1.79 $\mathring{A}$, which is about the same as in the bulk TiB_2 (1.73 $\mathring{A}$), but slightly larger than that of B sheet (1.67 $\mathring{A}$).[13,30] The vertical distance between Ti and B layer is 1.19 $\mathring{A}$, which is noticeably smaller than that in the bulk TiB_2 (1.575 $\mathring{A}$), indicating a much stronger interaction between Ti atoms and B layer. The binding energy between Ti and B layer is found to be E_b

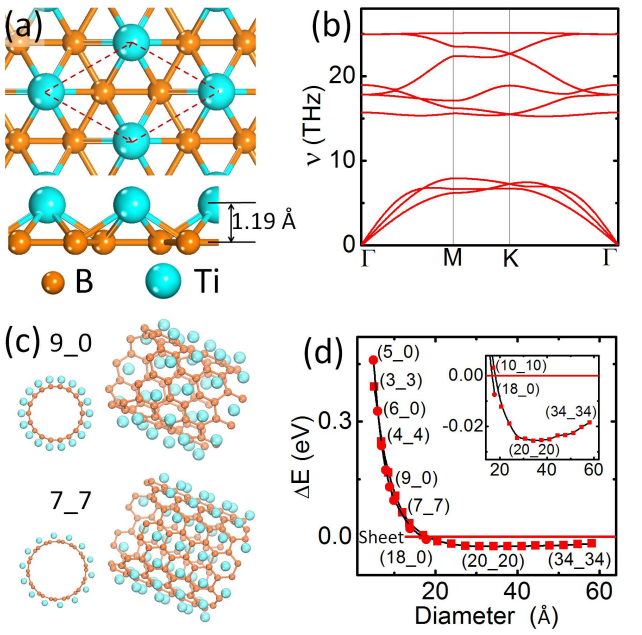

FIG. 1: (Color online) (a) Top and side view of m-TiB_2. (b) The phonon-dispersion curves of m-TiB_2. (c) Schematic structures for TiB_2 zigzag (9_0) and armchair (7_7) nanotubes. (d) Relative formation energies vs. the diameters of TiB_2 nanotubes (red dot/square corresponding to zigzag/armchair nanotubes), where the formation energy per TiB_2 unit cell is measured with respect to the m-TiB_2 (red line), insert figure shows the zoom-in of (d).

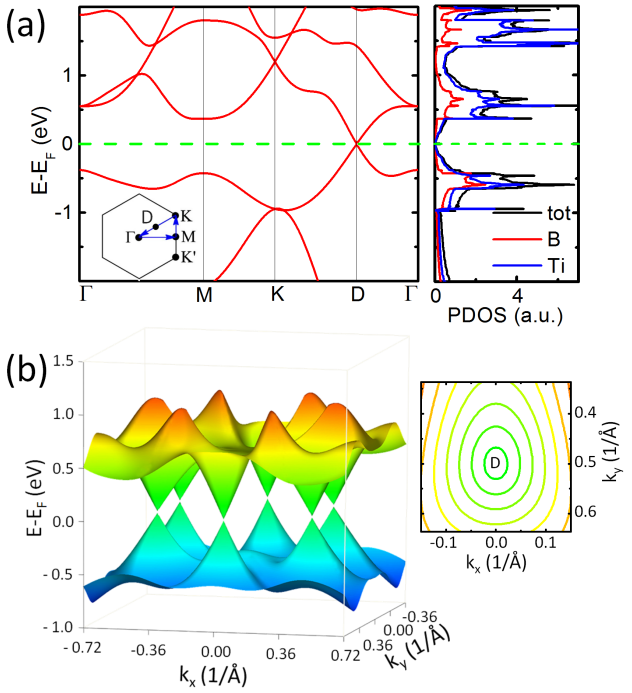

FIG. 2: (Color online) Electronic structures of m-TiB_2. (a) Band structure and PDOS. (b) 3-D valence and conduction bands and the Dirac cone in the vicinity of the Dirac point, the right panel of (b) shows the constant-energy contour for the valence band around one Dirac cone with an energy contour interval of 0.1 eV.

= -9.17 $eV/unitcell$ ($E_b = E_{tot} - E_{h-BS} - E_{Ti}$). We calculated the formation energy ($\triangle E$) per TiB_2 unit of m-TiB_2 relative to TiB_2 nanotubes. The TiB_2 nanotubes tend to bend towards the B side, as shown in Fig. 1(c). Fig. 1(d) shows that m-TiB_2 is more stable than small nanotubes with a diameter less than that of (18, 0) tube, but less stable than other larger ones. This indicates a bending instability of planar m-TiB_2 into tubular shape, an interesting point we will discuss further later. On the other hand, we also calculated phonon-dispersion curves of m-TiB_2, as shown in Fig. 1(b). The absence of imaginary frequencies demonstrates the dynamical stability of m-TiB_2.

The calculated band structures and projected density of states (PDOS) of m-TiB_2 are shown in Fig. 2(a). The main feature of band structure is two linear bands crossing at the E_F and located at an off-symmetry D $[(0.143, 0.286) * 2\pi/a)]$ point, between K and Γ point ($\sim$ 0.43 Γ_K). The PDOS show that the Dirac states near the E_F are predominantly contributed by Ti. We also plot the 3-D valence and conduction bands in Fig. 2(b), which clearly show the anisotropy of Dirac cone. The right panel of Fig. 2(b) shows the constant-energy contour for the valence band around one Dirac cone with an energy interval of 0.1 eV. The oval-shaped contour lines indicate that this Dirac cone is anisotropic with

TABLE I: On-site energy rectifications for different orbitals in Fig. 3(e) comparing with that in Fig. 3(a).

s	p_z	p_x	p_y	d_{z^2}	d_{xz}	d_{yz}	$d_{x^2-y^2}$	d_{xy}
-1.3	-1.05	-2	-2	1.6	0.8	0.8	-0.2	-0.2

the largest Fermi velocity of 0.57×10^6 m/s, and the linear dispersion maintains about $\pm$ 0.3 eV away from the Dirac point. Both the Fermi velocity and the energy range of Dirac state are close to one-half of those in freestanding graphene.[31] We also checked by including spin-orbital coupling, which causes a small spin splitting of bands, but without inducing a gap (See Fig. S4 in Supporting Information[41]).

To understand the origin of Ti orbital-originated Dirac states, band structures of a triangular Ti lattice (at the same lattice constants as in m-TiB_2) are calculated (blue line in Fig. 3(a)). Because of D_{6h} symmetry, Ti 3d orbitals split into e_1 (d_{xy}, $d_{x^2-y^2}$), e_1^* (d_{xz}, d_{yz}) and a_1^* (d_{z^2}) in the triangular lattice. Correspondingly, the band structures show five energy levels along the K-point: two couples of degenerate level e_1 and e_1^* and one a_1^*. By using Wannier90 package,[32] we fit a tight-binding (TB) Hamiltonian with maximally localized Wannier functions to the bands calculated by first principle method (red dots in Fig. 3(a)). They show very good agreement. Then, we

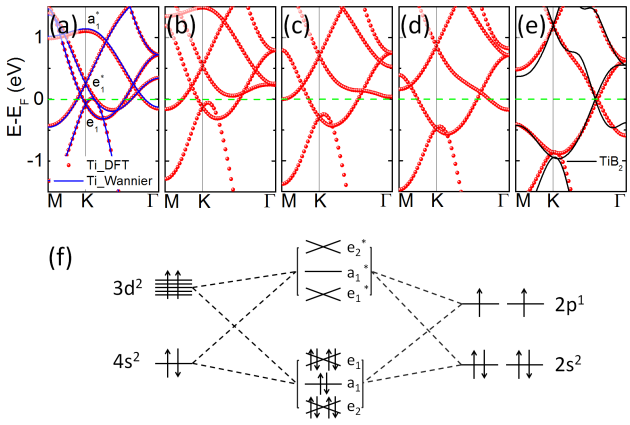

FIG. 3: (Color online) (a) First-principles and Wannier band structures for triangular Ti. (e) Band structures for triangular Ti at appropriate on-site energy (red points) and m-TiB_2 (black line). (b) - (d) Band structures at 20%, 40%, 60% on-site energy rectifications of that in Fig. 3(e). (f) Schematic drawing of the orbital hybridization between Ti and B. Each arrow denotes one electron with up or down spin.

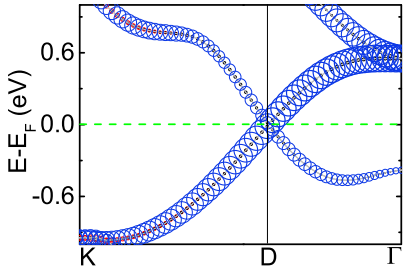

FIG. 4: (Color online) Projected band structures of m-TiB_2 near the Dirac point, where the radii of the blue (red, black) circles are proportional to the Ti d (B p_z, B $s + p_x + p_y$) character.

artificially tuned the on-site energies of the nine orbitals in the TB model (shown in Table 1), to reveal how the band structure of triangular Ti lattice would evolve [Fig. 3(b)-(d)] until with a chosen set of parameters it [red dots in Fig. 3(e)] would match closely with the band structure of m-TiB_2 [black line in Fig. 3(e)] around the Fermi level. This allows us to qualitatively confirm that the off-symmetry Dirac points/states come mainly from Ti d orbitals.[7] The calculated projected band structures [Fig. 4] also show that the bands near the Fermi level are mainly contributed by the Ti d orbitals. From Fig. 3(b)-(d), where 20%, 40%, and 60% of the on-site energy rectifications are taken in comparison with Fig. 3(e), respectively, we see that the Dirac bands arise from band splitting around the Fermi level. Because m-TiB_2 has C_{6v} symmetry, Ti $3d$ orbitals have similar splitting mode as that of triangular Ti (same energy sequence). As the triangular Ti lattice interact with the hexagonal B lattice in m-TiB_2, the B crystal field increases the band splitting of Ti lattice. Specifically, the effect of B lattice to the d orbitals of Ti is strongest in the z-direction. Consequently, the change of the on-site energies of d_{xz}, d_{yz} and d_{z^2} orbitals with z-components is much larger than those of d_{xy} and $d_{x^2-y^2}$ orbitals without z-components (Table 1).

Fig. 3(f) shows the hybridization between Ti and B schematically. The interaction between Ti sublattice and B sublattice leads to ten hybridized states, e_2, a_1, e_1, e_1^*, a_1^*, and e_2^*, respectively. e_1, e_1^* and a_1^* come from the triangular Ti sublattice [Fig. 5(a)], e_2, a_1 and e_2^* come from the sp^2 hybridizations in B sublattice [Fig. 5(b)];[33] e_2 and a_1 consist of s, p_x, and p_y characters (σ bands) of B, e_1 and e_1^* consist of d orbitals of Ti. Ten electrons, four from Ti and six from B, fully occupy the e_2, a_1 and e_1 states, leaving the five states with high energy empty. Thus, the interactions between Ti d orbitals and B p orbitals result in the appearance of Dirac point at the D point [Fig. 5(c)].

Most theoretically predicted and experimentally confirmed Dirac materials, such as graphene and topological insulators, are composed of p-orbital electrons. Within the single-particle band picture, there is no difference between the d-orbital and p-orbital linear Dirac band dispersions.[34,35] However, generally the d-orbital Dirac materials have stronger spin exchange interaction, larger spin-orbit coupling and more significant many-body correlation effect, which may yield new and rich physics, such as anomalous quantum Hall effect,[36] Mott insulator,[37] etc. Therefore, the prediction of new d-orbital Dirac materials is of both scientific and technological interests. Specifically, the d-orbital Dirac state predicted in the m-TiB_2 has several interesting features. 1) It has a highly anisotropic Dirac band structures (right part in Fig. 2(b)), which is desirable for manipulating the direction of electron propagation.[38,39] 2) It has a large

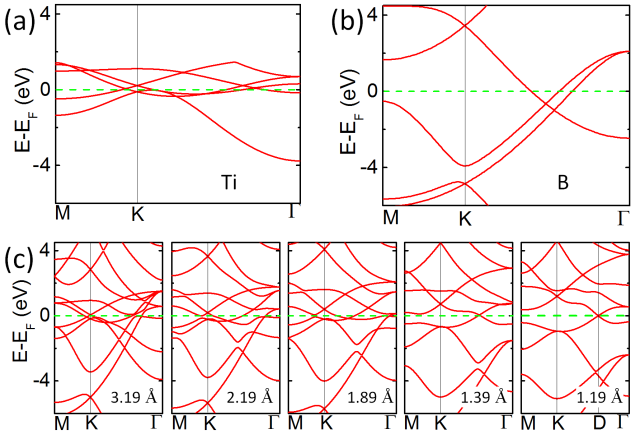

FIG. 5: (Color online) Band structures of (a) the triangular Ti, (b) hexagonal boron and (c) m-TiB_2 at different distances of Ti and boron layer (from 3.19$\AA$ to 1.19$\AA$).

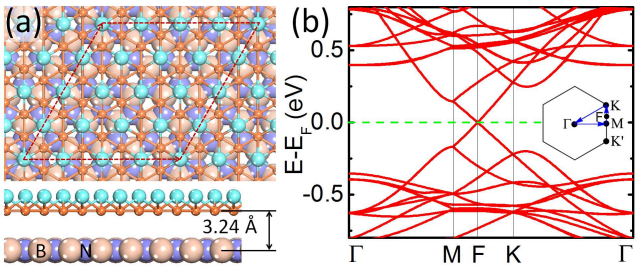

FIG. 6: (Color online) Relaxed structures (a) and band structures (b) of m-TiB_2 on h-BN.

Fermi velocity, which is comparable to the largest value obtained in the graphene.

For most TiB_2 nanotubes [with diameters larger than that of (18, 0) tube] are more stable than m-TiB_2 [Fig. 1(b)], the planar m-TiB_2 will bend into tubular shape. Thus, a planar m-TiB_2 needs to be stabilized on a substrate to overcome its bending moment.[40] Here, we use the h-BN as the substrate, according to two important reasons: 1) An infinite m-TiB_2 sheet or a wide enough m-TiB_2 nanoribbon can be stabilized on a h-BN substrate without bending. Based on stress calculations and following the analysis of Ref[40], we estimated that the minimum width of a m-TiB_2 nanoribbon is 3.22 nm to be stabilized. (see Supporting Information[41]) 2) Weak influence to the electronic properties of m-TiB_2 which can retain the Dirac states of m-TiB_2. According to the lattice constants of the h-BN and m-TiB_2, we choose a model which contains 4×4 m-TiB_2 on 5×5 h-BN, and fix the lattice of the h-BN. This model closely approximates the real system, for the lattice mismatch between m-TiB_2 and h-BN substrate is only 0.46%. The relaxed configuration of the m-TiB_2/h-BN system is shown in Fig. 6(a). We find that the distance between m-TiB_2 and h-BN substrate is about 3.24 $\mathring{A}$, and the adsorption energy is 94 meV/(Ti&2B). We also checked those results considering the van der Waals interactions (DFT+D/PBE). The resulting distance and adsorption energy is 3.08 $\mathring{A}$ and 435 meV/(Ti&2B). However, band structures remain the same,[41] suggesting weak interaction between m-TiB_2 and the substrate. Fig. 6(b) shows the band structure of the m-TiB_2/h-BN system. The linear dispersion relationship retains at the Dirac point. When m-TiB_2 is placed on the h-BN substrate, the periodicity is expanded into a 4×4 supercell for m-TiB_2 (See Fig. S3 in the Supporting Information). Consequently, the Dirac point moves to the F point in between M and K ($\sim 0.44\ M\_K$), which is folded from the D point of the m-TiB_2 band (Fig. 2(a)). Thus, we confirm that the Dirac states of m-TiB_2 can be retained on the h-BN substrate.

In Conclusion, by using first-principles calculations, m-TiB_2 is demonstrated to be Dirac material which is energetically and dynamically stable. Different from graphene, the Dirac cone is anisotropic with the largest Fermi velocity of $0.57\times10^6\ m/s$, and have the characters of transition metal d orbital. Further investigations show that the existence of d-band Dirac cones could be attributed to the d band splitting of the triangular Ti layers. Calculation of m-TiB_2 on h-BN substrate shows that the Dirac states are retained. Our study reveals a new kind of Dirac materials — metal borides.

We thank Q. B. Yan, M. Zhou, and F. Ye for helpful discussions. This work was partially supported by the Natural Science Foundation of China (Nos. 51325204, 61390501 and 51210003), the MOST 973 projects of China (No. 2011CB921702), the Chinese Academy of Sciences (CAS), Shanghai Supercomputer Center. Z. F. W and F. L. acknowledge support from DOE-BES (Grant No. DE-FG02-04ER46148).

*Corresponding author: sxdu@iphy.ac.cn
†Corresponding author: fliu@eng.utah.edu

[1] A. H. Castro Neto, N. M. R. Peres, K. S. Novoselov, and A. K. Geim, Rev. Mod. Phys. **81**, 109 (2012).

[2] K. S. Novoselov, A. K. Geim, S. V. Morozov, D. Jiang, M. I. Katsnelson, I. V. Grigorieva, S. V. Dubonos, and A. A. Firsov, Nature **438**, 197 (2005).

[3] A. K. Geim, and K. S. Novoselov, Nat. Mater. **6**, 183 (2007).

[4] K. K. Gomes, W. Mar, W. Ko, F. Guinea, and H. C. Manoharan, Nature **483**, 306 (2012).

[5] Y. D. Ma, Y. Dai, and B. B. Huang, J. Phys. Chem. L **4**, 2471 (2013).

[6] D. Malko, C. Neiss, F. Viñes, and A. Görling, Phys. Rev. Lett. **108**, 086804 (2012).

[7] Y. C. Li, P. C. Chen, G. Zhou, J. Li, J. Wu, B. L. Gu, S. B. Zhang, and W. H. Duan, Phys. Rev. Lett. **109**, 206802 (2012).

[8] H. J. Zhang, C. X. Liu, X. L. Qi, X. Dai, Z. Fang, and S. C. Zhang, Nat. Phys. **5**, 438 (2009).

[9] S. Cahangirov, M. Topsakal, E. Aktürk, H. Şahin, and S. Ciraci, Phys. Rev. Lett. **102**, 236804 (2009).

[10] X. F. Zhou, X. Dong, A. R. Oganov, Q. Zhu, Y. J. Tian, and H. T. Wang, Phys. Rev. Lett. **112**, 085502 (2014).

[11] Z. F. Wang, Z. Liu, and F. Liu, Nat. Commum. **4**, 1471 (2013).

[12] N. Gonzalez Szwacki, A. Sadrzadeh, and B. I. Yakobson, Phys. Rev. Lett. **98**, 166804 (2007).

[13] H. Tang, and S. Ismail-Beigi, Phys. Rev. Lett. **99**, 115501 (2007).

[14] S. Meng, and E. Kaxiras, Z. Y. Zhang, Nano Lett. **7**, 663 (2007).

[15] A. Quandt, A. Y. Liu, and I. Boustani, Phys. Rev. B **64**, 125422 (2001).

[16] S. Guerini, and P. Piquini, Microelectronics Journal **34**, 495 (2003).

[17] V. V. Ivanovskaya, A. N. Enjashin, A. A. Sofronov, Y. N. Makurin, N. I. Medvedeva, and A. L. Ivanovskii, Journal of Molecular Structure **625**, 9 (2003).

[18] P. H. Zhang, and V. H. Crespi, Phys. Rev. Lett. **89**, 056403 (2002).

[19] H. Tang, and S. Ismail-Beigi, Phys. Rev. B **80**, 134113 (2009).

[20] S. Y. Xie, X. B. Li, W. Q. Tian, N. K. Chen, X. L. Zhang, Y. L. Wang, S. B. Zhang, and H. B. Sun Phys. Rev. B **90**, 035447 (2014).

[21] C. Cepek, R. Macovez, M. San cortti, L. Prtaccia, R. Larciprete, S. Lizzt, and A. Goldoni, Appl. Phys. Lett. **85**, 976 (2004).

[22] G. Hilz, and H. Holleck, Int. J. of Refraxtory Metals Hard Materials **14**, 97 (1996).

[23] D. Vanderbilt, Phys. Rev. B **41**, 7892 (1990).

[24] G. Kresse, and J. Furthmuller, Phys. Rev. B **54**, 11169 (1996).

[25] P. E. Blöchl, Phys. Rev. B **50**, 17953 (1994).

[26] D. M. Ceperley, and B. J. Alder, Phys. Rev. Lett. **45**, 566 (1980).

[27] J. P. Perdew, and A. Zunger, Phys. Rev. B **23**, 5048 (1981).

[28] K. Parlinski, Z-. Q. Li, and Y. Kawazoe, Phys. Rev. Lett. **78**, 4063 (1997).

[29] A. Togo, F. Oba, and I. Tanaka, Phys. Rev. B **78**, 134106 (2008).

[30] X. B. Yang, Y. Ding, and J. Ni, Phys. Rev. B **77**, 041402(R) (2008).

[31] P. R. Wallace, Phys. Rev. **71**, 622 (1947).

[32] A. A. Mostofi, J. R. Yates, Y. -S Lee, I. Souza, D. Vanderbilt, and N. Marzari, Comput. Phys. Commun. **178**, 685 (2008).

[33] L. Z. Zhang, Q. B. Yan, S. X. Du, G. Su, and H. J. Gao, J. Phys. Chem. C **116**, 18202 (2012).

[34] Z. Liu, Z. F. Wang, J. W. Mei, Y. S. Wu, and F. Liu, Phys. Rev. Lett. **110**, 106804 (2013).

[35] M. Zhou, W. Ming, Z. Liu, Z. F. Wang, P. Li, and F. Liu, Epitaxial growth of large-gap quantum spin Hall insulator on semiconductor surface. Proc. Natl. Acad. Sci. in press.

[36] Z. F. Wang, Z. Liu, and F. Liu, Phys. Rev. Lett. **110**, 196801 (2013).

[37] I. I. Mazin, H. O. Jeschke, F. Lechermann, H. Lee, M. Fink, R. Thomale, and R. Valenti, Nature Commun. **5**, 4261 (2014).

[38] C. H. Park, L. Yang, Y. W. Son, M. L. Cohen, and S. G. Louie, Nature Phys. **4**, 213 (2008).

[39] Z. F. Wang, and F. Liu, ACS Nano **4**, 2459 (2010).

[40] D. C. Yu, and F. Liu, Nano Lett.**10**, 3046 (2007).

[41] See Supplemental Material at http://link.aps.org/supplemental/10.1103/PhysRevB for calculation details about the minimum width of m-TiB_2 nanoribbon on h-BN, the calculation results of m-TiB_2/h-BN system by using the DFT+D/PBE method, the band folding from 1×1 m-TiB_2 to 4×4 m-TiB_2, and band structures of m-TiB_2 with spin-orbital coupling.